Supporting Materials for

Aligning Curved Stacking Bands to Simultaneously Strengthen and Toughen Lamellar Materials

Yanqiu Jiang[a, b#], Fan Guo[a, d#], Jiacheng Zhang[c], Zhen Xu[a*], Fang Wang[a], Shengying Cai[a], Yingjun Liu[a], Yi Han[e], Chen Chen[e], Yilun Liu[c*], Weiwei Gao[a] & Chao Gao[a*]

[a] MOE Key Laboratory of Macromolecular Synthesis and Functionalization, Department of Polymer Science and Engineering, Key Laboratory of Adsorption and Separation Materials & Technologies of Zhejiang Province, Zhejiang University, 38 Zheda Road, Hangzhou 310027, China.

[b] State Key Lab of Chemical Engineering, College of Chemical and Biological Engineering, Zhejiang University, Hangzhou 310027, China.

[c] State Key Laboratory for Strength and Vibration of Mechanical Structures, School of Aerospace, Xi'an Jiaotong University, 710049 Xi'an, P. R. China.

[d] National Special Superfine Powder Engineering Research Center, Nanjing University of Science and Technology, 1 Guanghua Road, Nanjing 210094, P. R. China.

[e] Hangzhou Gaoxi Technology Co., Ltd., Hangzhou 310027, China.

[#] Y. Jiang and F. Guo contribute equally to this work.

*Corresponding author Email: zhenxu@zju.edu.cn; yilunliu@mail.xjtu.edu.cn; chaogao@zju.edu.cn

This PDF file includes:

Fig. S1 to S18

Table S1

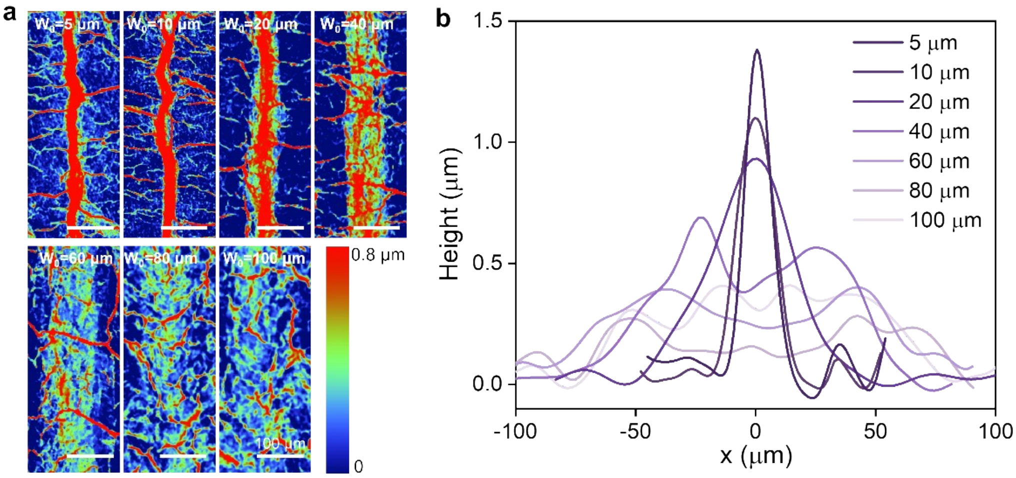

Fig. S1 (**a**) WLI images of the surface morphology of CS bands constructed by probes with different diameters. (**b**) Typical section profiles of CS bands constructed by probes with different diameters.

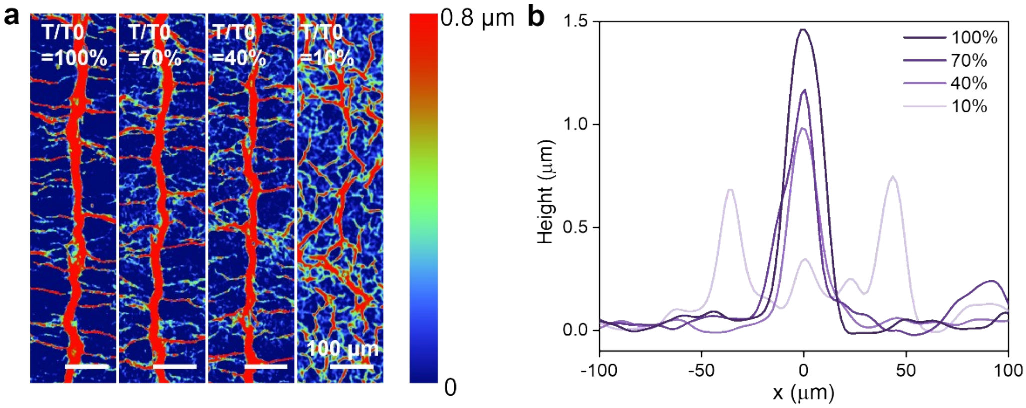

Fig. S2 (**a**) WLI images of the surface morphology of CS bands constructed by probes with different relative immerse depths. (**b**) Typical section profiles of CS bands constructed by probes with different relative immerse depths.

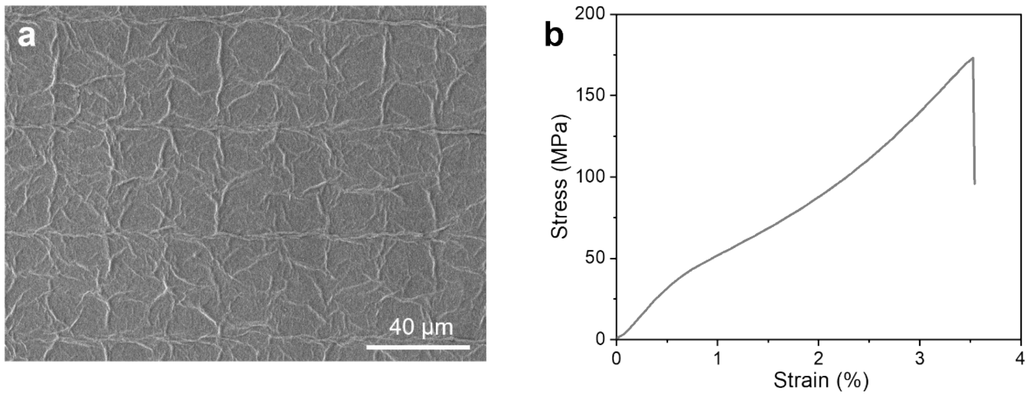

Fig. S3 (**a**) SEM images of the surface morphology of GOF films with biaxial aligned CS bands. (**b**) Stress-strain curves of GOF films with biaxial aligned CS bands.

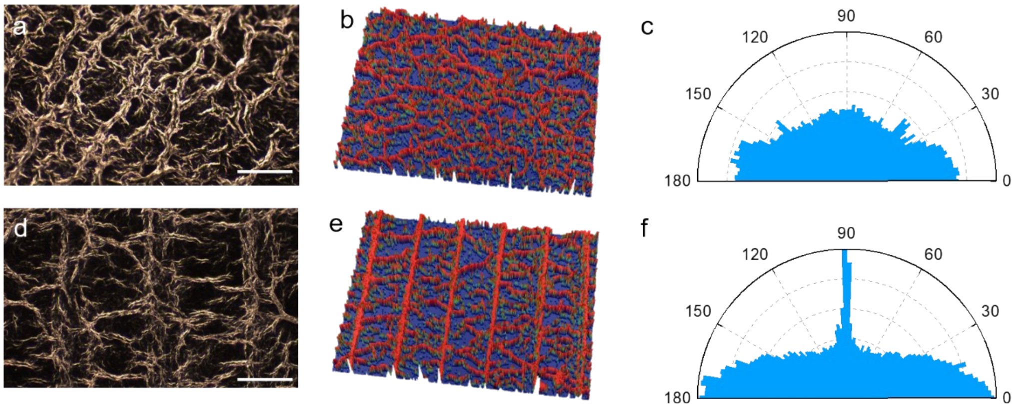

Fig. S4 (**a-c**) Dark field optical image (a), WLI image (b) and orientation distribution (c) of the surface wrinkles for GF. (**d-f**) Dark field optical image (d), WLI image (e) and orientation distribution (f) of the surface wrinkles for G200. (Scale bars: a, d 100 μm)

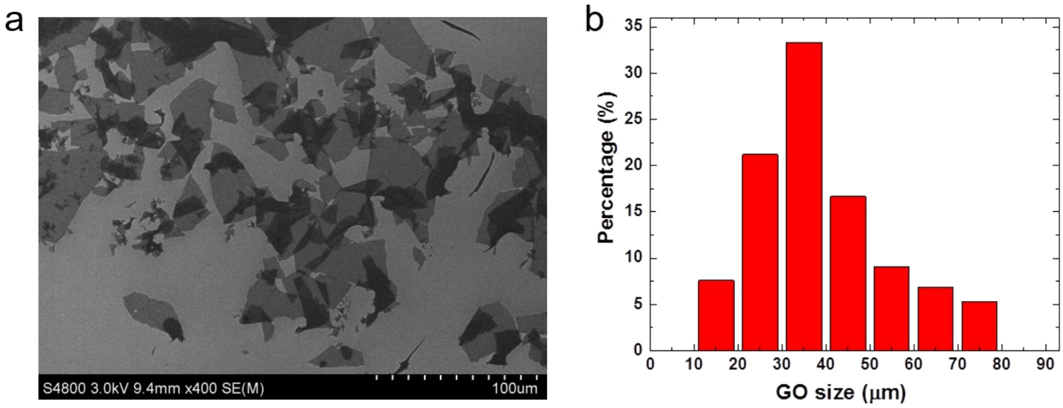

Fig. S5 (**a**) SEM images of GO sheets. (**b**) Statistics of lateral size distribution of GO sheets.

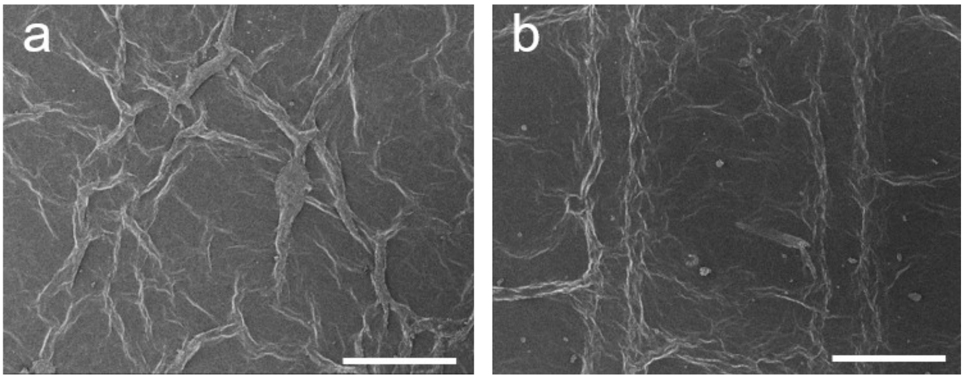

Fig. S6 SEM images of the surface wrinkles for GF (**a**) and G200 (**b**). (Scale bars: a, b 100 μm)

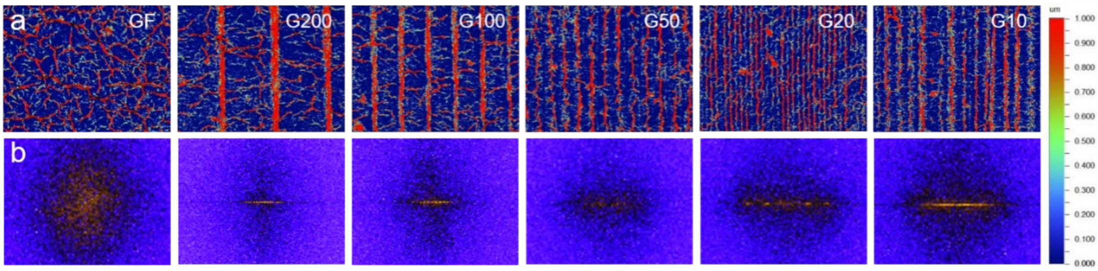

Fig. S7 (**a**) WLI images of the surface wrinkle of GFs with different *d*. (**b**) Their corresponding FFT spectra.

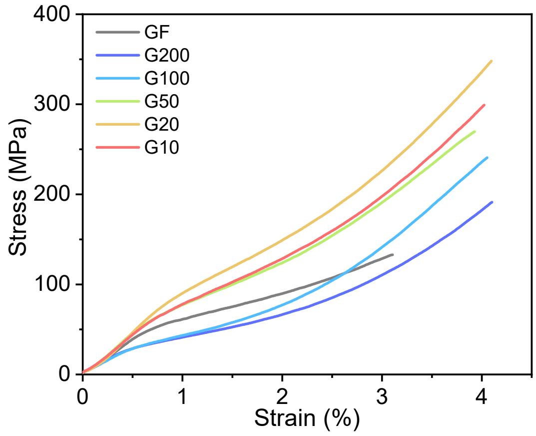

Fig. S8 Uniaxial tensile stress-strain curves for GF, G200, G100, G50, G20 and G10 films.

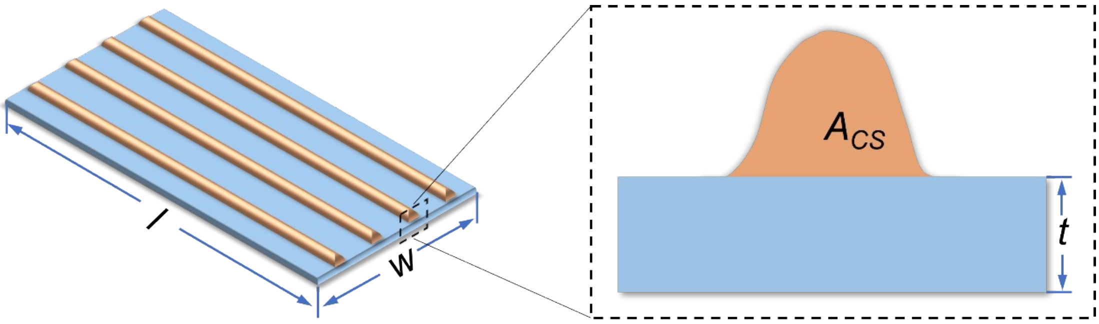

Fig. S9 Schematic diagram of the calculation process of cross-sectional areas (*A*) for GOF with aligned ridges.

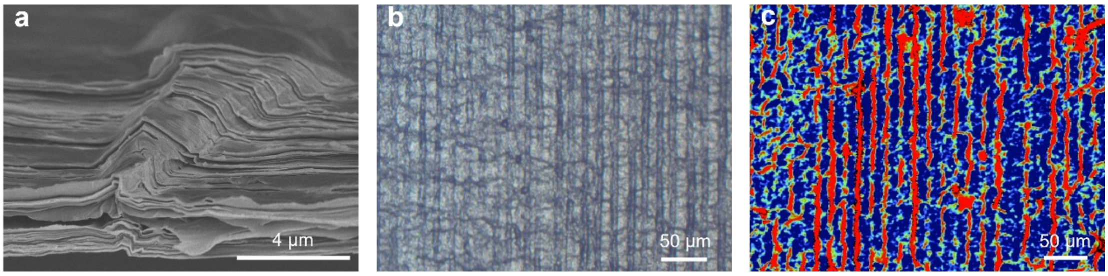

Fig. S10 (**a**) SEM images of the section morphology of CS bands after prolonged stretching. (**b, c**) POM and WLI images of the surface morphology of CS bands after prolonged stretching.

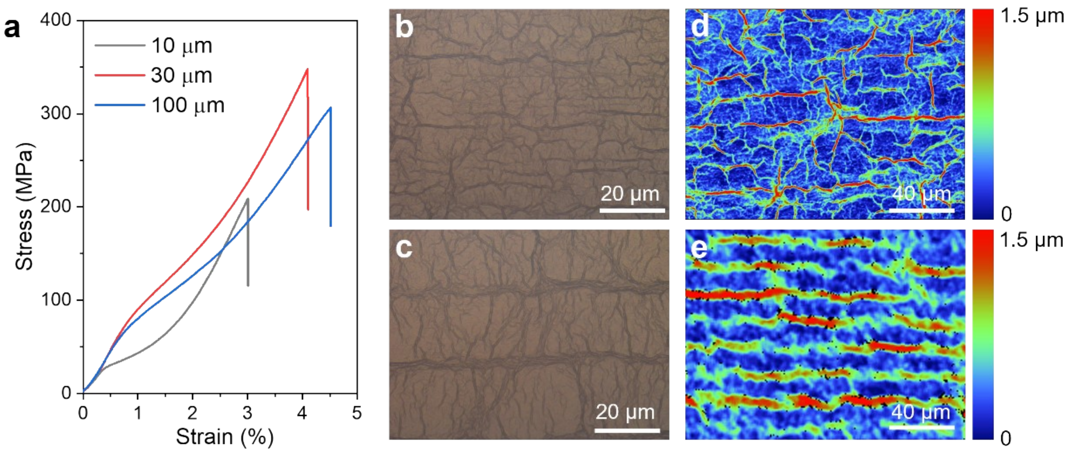

Fig. S11 (**a**) Stress-strain curves of G20 films made of GO sheets with different lateral sizes. (**b, c**) POM images of the surface morphology of G20 films made of GO sheets with lateral sizes of (b) 10 μm and (c) 100 μm. (**d, e**) WLI images of the surface morphology of G20 films made of GO sheets with lateral sizes of (d) 10 μm and (e) 100 μm.

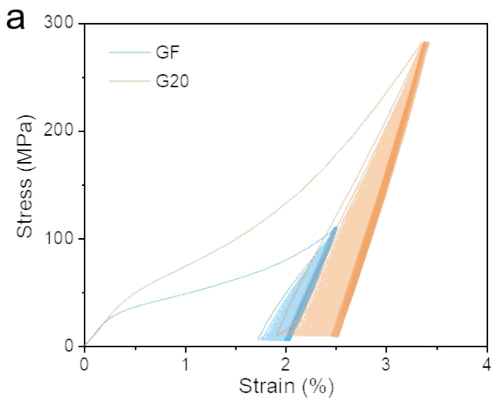

Fig. S12 Tensile stress-strain curves of GF and G20 films during 1000 tensile loading-unloading cycles.

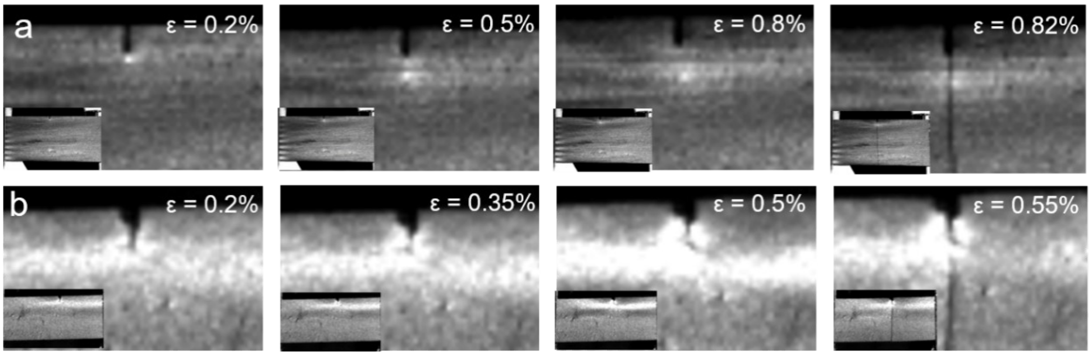

Fig. S13 Images taken by high-speed camera to track the fracture process of G20 (**a**) and GF (**b**) films.

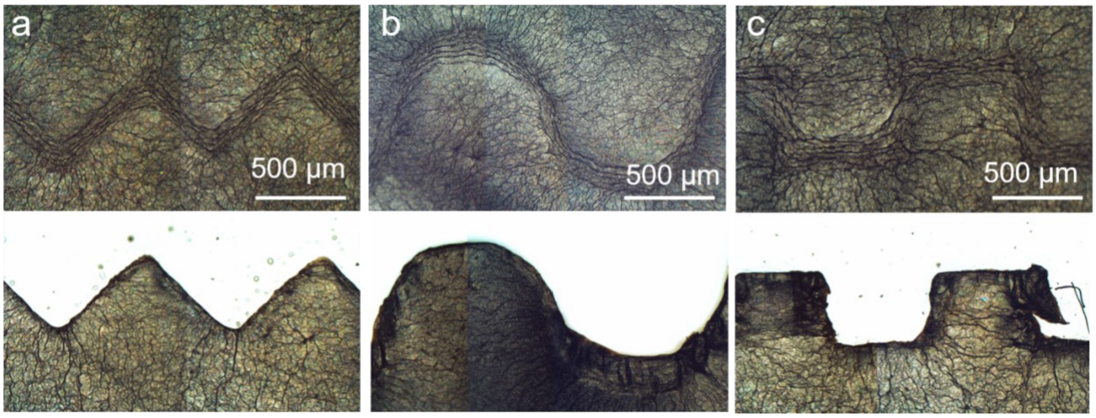

Fig. S14 Optical images of GFs with CS bands aligned in (**a**) jagged, (**b**) wavy, and (**c**) step-like manner and their corresponding fracture surface.

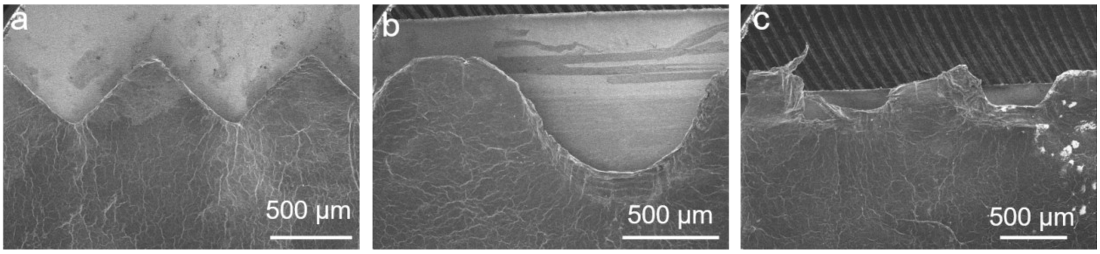

Fig. S15 SEM images of fracture surface of GFs with CS bands aligned in (**a**) jagged, (**b**) wavy, and (**c**) step-like manner.

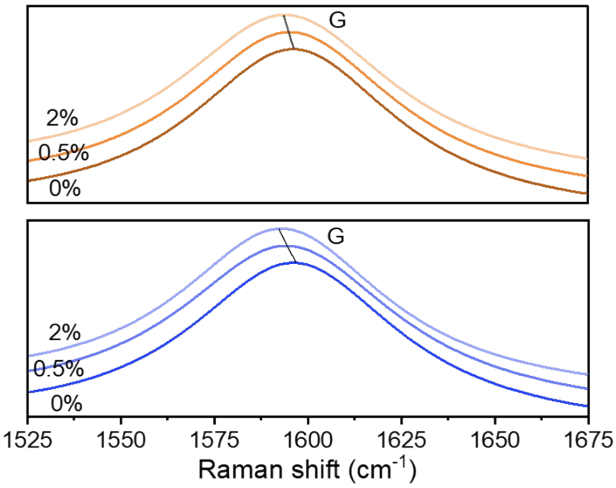

Fig. S16 The Raman shift of G peak in CS bands (top, orange) and plain area (bottom, blue) for G20 films under different tensile strains.

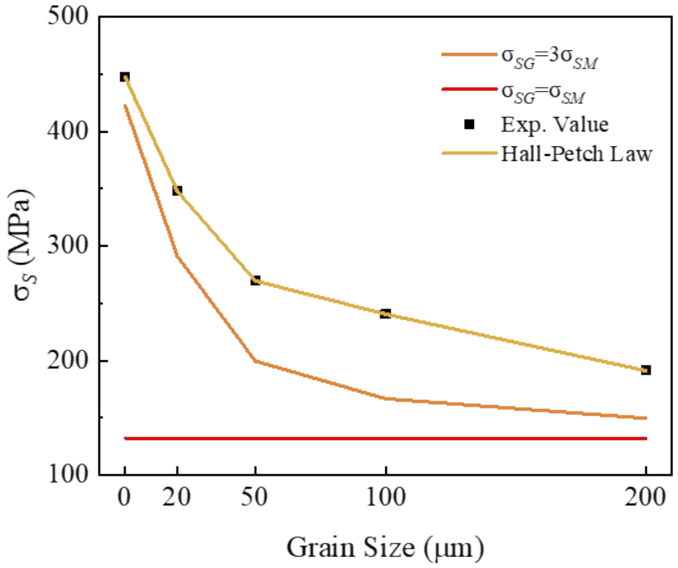

Fig. S17 Grain size effect of LMs and CS bands enhancement effect. From the perspective of composite, the mixture strength is expressed: $\bar{\sigma}_S = \sigma_{SG} f_G + \sigma_{SM} f_M$, where f_G is the CS bands volume fraction, f_M is the membrane volume fraction, σ_{SG} is the fracture strength of the CS bands, and σ_{SM} is the fracture strength of the membrane. Even we assume the strength of CS bands is 3 times of the membrane strength (we think the ridge strength is only comparable to the membrane strength due to the similar constituent and structure), the predicted fracture strength is still much smaller than the experiments.

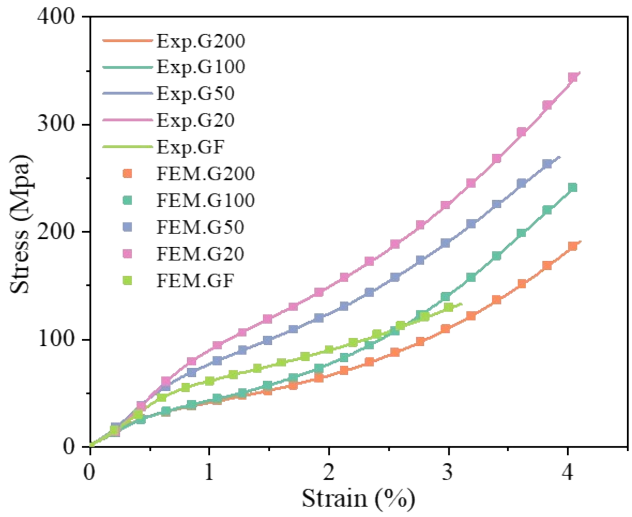

Fig. S18 Comparison of FEM results with experimental stress-strain curves for different GFs.

Table S1 The mechanical property data of our ridged GFs and other GO based films.

Sample	Strength (MPa)	Toughness (MJ m^{-3})	Reference
Nacre	200	2.6	*Nat. Mater.* **2015**, *14,* 23
GO-PVA	80.2	0.1	*Adv. Funct. Mater.* **2010**, *20*, 3322
GO-PMMA	148.3	2.35	*Adv. Funct. Mater.* **2010**, *20*, 3322
GO-Al_2O_3-PVA	143	9.2	ACS Appl. Mater. Interfaces 2015, *7*, 9281
GO-SA	240	1.3	*Nano Res.* **2016**, *9*, 735
GO-Ca^{2+}	125.8	0.31	*ACS Nano*, **2008**, *2*, 572
GO-Mg^{2+}	80.6	0.13	*ACS Nano*, **2008**, *2*, 572
GO-Al^{3+}	100.5	0.23	*Nat. Chem.* **2015**, *7*, 166
GO-Zn^{2+}	142.2	0.32	*Chem. Commun.* **2015**, *51*, 2671
GO-GA	101	0.3	*ACS Nano*, **2011**, *5*, 2134
GO-borate	185	0.14	*Adv. Mater.* **2011**, *23*, 3842
GO-PEI	209.9	0.23	*Adv. Mater.* **2013**, *25*, 2980
GO-PCDO	129.6	3.91	*Angew. Chem., Int. Ed.,* **2013**, *52*, 3750
GO-PAA	91.9	0.21	*J. Phys. Chem. C,* **2009**, *113*, 15801
GO-PDA	266	4.92	*Adv. Funct. Mater.* **2017**, *27*, 1605636
GO-CNC	490	3.9	*Adv. Mater.* **2016**, *28*, 1501
GO-annealing	211	3.91	*Adv. Mater.* **2014**, *26*, 7588
GF	133	2.35	This work
G20	348	6.64	This work